

Fluence dependent femtosecond quasi-particle and Eu^{2+} -spin relaxation dynamics in $\text{EuFe}_2(\text{As,P})_2$

A. Pogrebna,¹ T. Mertelj,^{1,2,*} G. Cao,³ Z. A. Xu,³ and D. Mihailovic^{1,2}

¹Complex Matter Dept., Jozef Stefan Institute, Jamova 39, Ljubljana, SI-1000, Ljubljana, Slovenia

²CENN Nanocenter, Jamova 39, Ljubljana SI-1000, Slovenia

³Department of Physics, Zhejiang University, Hangzhou 310027, People's Republic of China

(Dated: 1st August 2016)

We investigated temperature and fluence dependent dynamics of the time resolved optical reflectivity in undoped spin-density-wave (SDW) and doped superconducting (SC) $\text{EuFe}_2(\text{As,P})_2$ with emphasis on the ordered Eu^{2+} -spin temperature region. The data indicate that the SDW order coexists at low temperature with the SC and Eu^{2+} -ferromagnetic order. Increasing the excitation fluence leads to a thermal suppression of the Eu^{2+} -spin order due to the crystal-lattice heating while the SDW order is suppressed nonthermally at a higher fluence.

I. INTRODUCTION

In the iron-based superconductors family^{1,2} $\text{EuFe}_2(\text{As,P})_2$ ³ and $\text{Eu}(\text{Fe,Co})_2\text{As}_2$ ⁴ offer an interesting experimental possibility to study the competition between the ferromagnetic (FM) and superconducting (SC) order parameters that can lead to nonuniform magnetic and SC states⁴⁻⁷, since the optimal critical temperature $T_c \sim 28$ K⁸ is comparable to the Eu^{2+} -spin ordering temperatures $T_M \sim 20$ K.^{3,9}

While no coherent picture of Eu^{2+} -spin ordering upon P or Co doping exists^{4,10-12}, a pure FM ordering¹² coexisting with superconductivity was reported by Nandi *et al.*¹² in $\text{EuFe}_2(\text{As}_{0.85}\text{P}_{0.15})_2$. Our recent transient magneto-optical spectroscopy study¹³ also points towards the simple FM Eu^{2+} -spin order in the superconducting $\text{EuFe}_2(\text{As}_{1-x}\text{P}_x)_2$ with a slow energy transfer between the FeAs-plane quasiparticles and Eu^{2+} spins indicating a weak magnetic-dipole dominated coupling between the SC and FM order parameters.

Here we extend our previous transient reflectivity study¹³ first focusing briefly on the spin-density-wave dominated part of the phase diagram followed by a study of the superconducting phase-diagram region at varying excitation density to study a suppression of the coexistent orders on an ultrafast timescale.

II. EXPERIMENTAL

A. Samples

Single crystals of $\text{EuFe}_2(\text{As}_{1-x}\text{P}_x)_2$ were grown by the flux method, similar to the previous report¹⁴. Small Eu chunks and powders of Fe, As and P (Alfa Aesar, > 99.9%) were mixed together in the molar ratio of $\text{Eu}:\text{Fe}:\text{As}:\text{P} = 1:5:5(1-x):5x$ (x is the nominal P content) and sealed in an evacuated quartz ampule. After heating the mixture up to 973 K for 24 hours, the obtained precursor was thoroughly ground before being loaded into an alumina crucible. The crucible was then sealed by arc welding in a tube made of stainless steel under atmo-

sphere of argon, and then heated up to 1573 K over 10 hours in a muffle furnace filled with argon. After holding at 1573 K for 5 hours, the furnace was cooled down to 1223 K at the rate of 5 K/h. followed by switching off the furnace. Large crystals with size up to $4 \times 4 \times 0.6$ mm³ could be harvested.

The as-grown crystals were characterized by X-ray diffraction, which showed good crystallinity as well as single “122” phase. The exact composition of the crystals was determined by energy dispersive X-ray spectroscopy affiliated to a field-emission scanning electron microscope (FEI Model SIRION). The measurement precision was better than 5% for the elements measured.

The out-of-plane magnetic susceptibilities shown in Fig. 1 are consistent with previous results.^{11,15} From the susceptibility we infer Eu^{2+} spin ordering temperatures $T_N = 19$ K and $T_C = 17.6$ K in EuFe_2As_2 (Eu-122) and $\text{EuFe}_2(\text{As}_{0.81}\text{P}_{0.19})_2$ (EuP-122), respectively. EuP-122 also shows the onset of superconductivity at $T_c = 22.7$ K.

B. Optical setup

Measurements of the photoinduced reflectivity, $\Delta R/R$, were performed using the standard pump-probe technique, with 50 fs optical pulses from a 250-kHz $\text{Ti}:\text{Al}_2\text{O}_3$ regenerative amplifier seeded with an $\text{Ti}:\text{Al}_2\text{O}_3$ oscillator. We used the pump photons with both, the laser fundamental ($\hbar\omega_P = 1.55$ eV) and the doubled ($\hbar\omega_P = 3.1$ eV) photon energy, and the probe photons with the laser fundamental $\hbar\omega_{pr} = 1.55$ eV photon energy. When using the doubled photon energy the scattered pump photons were rejected by long-pass filtering, while an analyzer oriented perpendicularly to the pump beam polarization was used for rejection in the case of the degenerate pump and probe photon energies. The pump and probe beams were nearly perpendicular to the cleaved sample surface (001) with polarizations perpendicular to each other and oriented with respect to the crystals to obtain the maximum/minimum amplitude of the sub-picosecond $\Delta R/R$ at low temperatures. The pump beam diameters

were, depending on experimental conditions, in 50-100 μm range with somewhat smaller probe beam diameters.

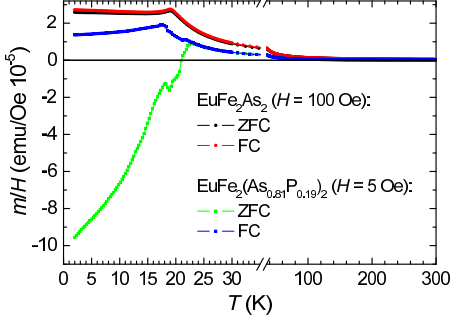


Figure 1. (Color online) Magnetic moment along the c -axis as a function of temperature for both, field cooled (FC) and zero field cooled (ZFC) cases.

III. RESULTS

A. Anisotropy of the $\Delta R/R$ transients

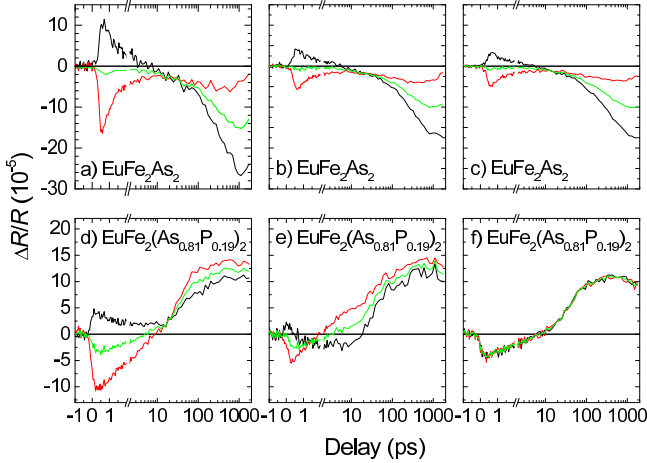


Figure 2. (Color online) Variation of the transients across the sample surface at $T = 1.5$ K and 1.5-eV pump-photon energy in EuFe_2As_2 (a), (b), (c) and $\text{EuFe}_2(\text{As}_{0.81}\text{P}_{0.19})_2$ (d), (e), (f). Black and red lines are the transients for \mathcal{P}^+ and \mathcal{P}^- probe polarizations, respectively, while green lines are the corresponding averages. The pump fluences used were $\mathcal{F} \sim 10 \mu\text{J}/\text{cm}^2$ (a) and $\mathcal{F} \sim 3 \mu\text{J}/\text{cm}^2$ (b)-(f).

At low temperatures we observe a 2-fold rotational anisotropy of the response with respect to the probe polarization at both doping levels. In the absence of information about the in-plane crystal axes orientation we denote the probe-polarization orientation according to the

polarity of the observed sub-picosecond low- T response as \mathcal{P}^+ and \mathcal{P}^- .

In EuP-122 we found a significant variation of the anisotropy, as well as the transients shape, across the sample surface. On the other hand, as shown in Fig. 2, there is almost no variation of the \mathcal{P}^+ , \mathcal{P}^- averaged transients indicating that the anisotropy variation is due to the twin domain structure on the length scale of the probe-beam diameter of $\sim 50 \mu\text{m}$. For all other measurements we therefore measured the single domain response by choosing the position on the sample surface with maximal anisotropy.

B. Response in the SDW state

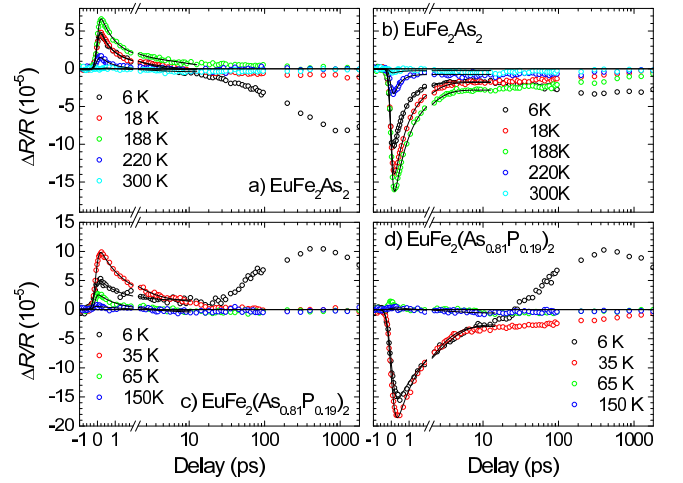


Figure 3. (Color online) Photoinduced reflectivity transients at $\mathcal{F} \sim 10 \mu\text{J}/\text{cm}^2$ and 3.1 eV pump photon energy in EuFe_2As_2 (a), (b) and $\text{EuFe}_2(\text{As}_{0.81}\text{P}_{0.19})_2$ (c), (d). Left and right panels correspond to \mathcal{P}^+ and \mathcal{P}^- polarizations, respectively. The thin lines are the finite-excitation-pulsewidth double-exponential relaxation fits.¹⁶

1. Experimental data

In Fig. 3 we show $\Delta R/R$ transients at a few characteristic temperatures for both samples. Starting at $T = 300$ K we observe sub-picosecond isotropic transients in both samples consistent with previous results in related iron-based pnictides.¹⁶⁻¹⁸ With decreasing T the 2-fold anisotropy appears below ~ 250 K in Eu-122 and ~ 190 K in EuP-122. The appearance of the anisotropy is followed by a strong increase of the amplitude of the sub-picosecond response peaking near the onset of the Fe- d SDW order at 188 K in Eu-122 and at significantly lower $T \sim 35$ K in EuP-122 as shown in Fig. 4. The initial-picosecond-relaxation decay time, obtained from double-exponential fits shown in Fig. 3, shows a divergence-like

sample	$2\Delta(0)/k_B T_{\text{SDW}}$	g_{ph}
EuFe ₂ As ₂	12 ± 7	2.2 ± 1
EuFe ₂ (As _{0.81} P _{0.19}) ₂	5 ± 1	2.9 ± 1.7

Table I. The SDW charge gap magnitudes and the relative effective number of involved bosons as obtained from the fits to the data, described in detail in Ref. [19] and shown in Fig. 4 (c), (d).

peak at the magneto-structural SDW transition in Eu-122 while in EuP-122 it only shows a plateau with no peak, concurrent with the amplitude maximum around ~ 35 K. In Eu-122 the initial picosecond relaxation also appears almost twice faster than in EuP-122.

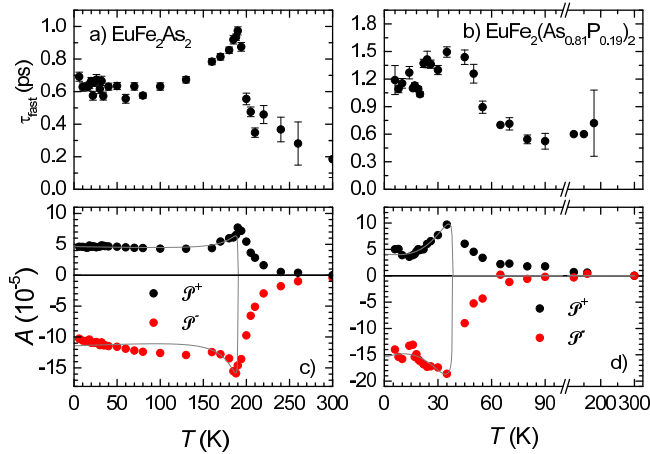


Figure 4. (Color online) The relaxation time (a), (b) and amplitude (c), (d) of the sub-picosecond response as a function of temperature in EuFe₂As₂, (a), (c) and EuFe₂(As_{0.81}P_{0.19})₂, (b), (d) at $\mathcal{F} \sim 10 \mu\text{J}/\text{cm}^2$ and 3.1 eV pump photon energy. The full lines in are the bottleneck model^{16,19} fits discussed in text.

2. Discussion

The initial fast relaxation in the undoped SDW state has been analysed previously in terms of the magnon-bottleneck model.^{16,17,19} The data in Eu-122 are consistent with our broad-band probe results on the same samples,¹⁹ with the bottleneck-fit parameters shown in Table I.

The T -dependent relaxation in doped EuP-122 is qualitatively similar to Eu-122 suggesting the presence of the magnetostructural/SDW transition at $T_{\text{SDW}} \sim 35$ K, consistent with the reported phase diagrams.^{8,12,20} The decrease of the relative charge gap magnitude $2\Delta(0)/k_B T_{\text{SDW}}$ with SDW suppression upon P doping is similar as in the Ba(Fe,Co)₂As₂.¹⁶ Despite the effective SDW induced charge-gap magnitude in EuP-122 ($2\Delta(0) \approx 15$ meV, see Table I) falls well into the phonon energy range no significant increase of the relative number of bottleneck bosons

is observed suggesting that the electron-phonon coupling in the vicinity of the SDW induced gap is weak.

In both samples we observe similarly to Ba(Fe,Co)₂As₂¹⁶ a 4-fold symmetry breaking at temperatures significantly exceeding the corresponding magnetostructural transition temperatures which we associate with nematic fluctuations^{21–23}.

C. Response related to Eu²⁺ spin ordering

Concurrently with the Eu²⁺-spin ordering^{10,24} below $\sim 17 - 19$ K we observe¹³ in both samples appearance of another much slower relaxation component with a risetime of ~ 1 ns in Eu-122 and ~ 100 ps in EuP-122 (at $T = 1.5$ K) and the decay time beyond the experimental delay range (see Fig. 3). In Eu-122 the slow component is rather anisotropic, while in EuP-122 it appears almost isotropic at the chosen pump fluence.

Since the T - and B -dependence of this component have been already analysed and discussed previously¹³ we omit further details here focusing on further aspects of our data not discussed elsewhere.

1. Pump fluence dependence

The pump fluence dependence of the response at low T is shown in Figs. 5 and 6 for Eu-122 and EuP-122, respectively. While in Eu-122 the sub-picosecond response shows only a slightly sublinear \mathcal{F} -dependence (see Fig. 7) with almost \mathcal{F} -independent sub-picosecond relaxation time in the full fluence range, the slow part of the response shows a clear sublinear \mathcal{F} -dependence already at $\mathcal{F} \sim 10 \mu\text{J}/\text{cm}^2$. The saturation above $\mathcal{F} \sim 100 \mu\text{J}/\text{cm}^2$ is concurrent with an increase of the risetime beyond the experimental delay range of 1.7 ns at the highest fluences. Interestingly, independently of \mathcal{F} all \mathcal{P}^+ transients cross zero at ~ 3 -ps delay. Above $\mathcal{F} \sim 50 \mu\text{J}/\text{cm}^2$ an additional dynamics with a risetime on ~ 10 -ps and decay on a few-100-ps timescale becomes apparent.

In superconducting EuP-122 the \mathcal{F} -dependence of the transients appears even more complex. There is a marked nonlinear behavior in both, the picosecond and nanosecond responses. The amplitude of the initial fast response with a sub-ps risetime is linear up to $\sim 20 \mu\text{J}/\text{cm}^2$ and clearly saturates above $\sim 50 \mu\text{J}/\text{cm}^2$ (see Fig. 8).

The shape of the fast response, contrary to Eu-122, strongly depends on the fluence. For the \mathcal{P}^- polarization at the lowest \mathcal{F} we observe after the initial sub-ps negative transient an increase of the signal with zero crossing to an intermediate value on a timescale of 2 ps followed by a partial decay on a ~ 10 -ps timescale with no further decay within our time window (see Fig. 6). With increasing \mathcal{F} the initial increase becomes slower with zero crossing moving beyond ~ 100 ps, while the 10-ps partial decay vanishes above $\mathcal{F} \sim 5 \mu\text{J}/\text{cm}^2$.

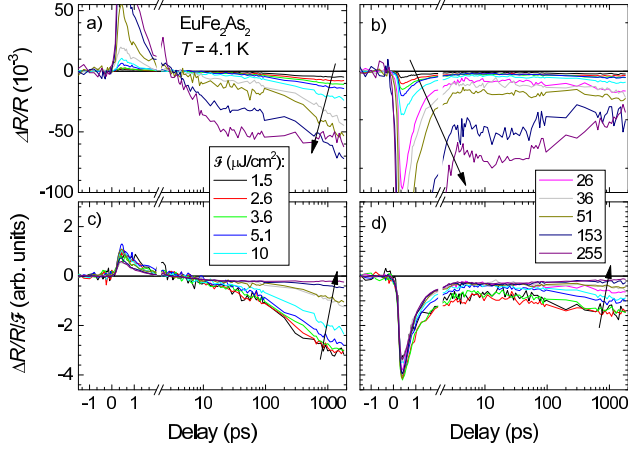


Figure 5. (Color online) The low- T transients in EuFe_2As_2 at different fluences for \mathcal{P}^+ , (a), and \mathcal{P}^- , (b) probe polarizations and 1.55-eV pump photon energy. To emphasize the low- \mathcal{F} region the \mathcal{F} -normalized transients from panels (a) and (b) are shown in (c) and (d), respectively. The arrows indicate the direction of increasing fluence. Note that the overlap of the \mathcal{F} -normalized scans indicates a linear dependence.

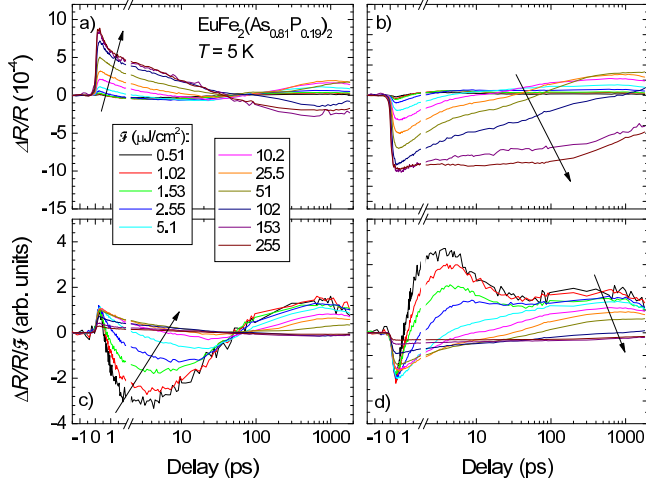


Figure 6. (Color online) The low- T transients in $\text{EuFe}_2(\text{As}_{0.81}\text{P}_{0.19})_2$ at different fluences for \mathcal{P}^+ , (a), and \mathcal{P}^- , (b), probe polarizations and 1.55-eV pump photon energy. To emphasize the low- \mathcal{F} region the \mathcal{F} -normalized transients from panels (a) and (b) are shown in (c) and (d), respectively. Arrows indicate the direction of increasing fluence. Note that the overlap of the \mathcal{F} -normalized scans indicates a linear dependence.

For the \mathcal{P}^+ polarization the initial-few-ps response at low \mathcal{F} is similar to the \mathcal{P}^- polarization response with the opposite sign. At longer delays, beyond ~ 10 ps, however, the slow component is observed causing a second zero crossing with a characteristic risetime of ~ 200 ps at the lowest \mathcal{F} , which increases beyond the experimental delay range with increasing \mathcal{F} . As a result, $\Delta R/R$ appears rather isotropic at long delays.

The slow response is linear in \mathcal{F} up to $\sim 10 \mu\text{J}/\text{cm}^2$

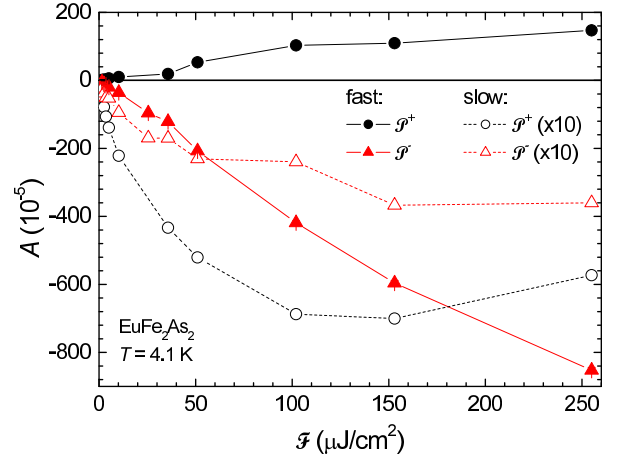


Figure 7. (Color online) The amplitude of the short delay extrema and the amplitude at the longest delay of the transients in EuFe_2As_2 as functions of fluence at $T = 6$ K and 1.55-eV pump photon energy.

at $T = 1.5$ K showing saturation with increasing \mathcal{F} (see inset to Fig. 8). The amplitude of the initial fast relaxation saturates above $\mathcal{F} \sim 50 \mu\text{J}/\text{cm}^2$. Concurrently it slows down (Fig. 6) and starts to overlap with the onset of the slow one.

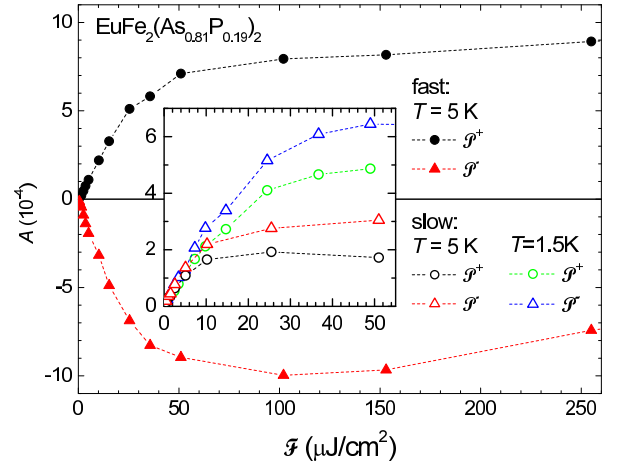


Figure 8. (Color online) The amplitude of the sub-picosecond extrema of the transients in $\text{EuFe}_2(\text{As}_{0.81}\text{P}_{0.19})_2$ as functions of fluence at $T = 5$ K and 1.55-eV pump photon energy. The inset shows the amplitude of the long delay extrema at low fluences including the data measured at 1.5 K.

Above $\mathcal{F} \sim 100 \mu\text{J}/\text{cm}^2$ the shape of the slow response shows an apparent qualitative change without the long delay zero crossings in both polarizations resulting in a change of sign of the nanosecond-timescale transient reflectivity.

2. Discussion

On the basis of a detailed temperature and magnetic field dependence we have shown previously¹³ that the slow component can be associated with Eu^{2+} spin demagnetization in both the AFM and FM states. The saturation of the slow response at high excitation fluences can therefore be associated with a complete suppression of the Eu^{2+} sublattice magnetizations due to the lattice temperature rise above the magnetic ordering temperatures. Taking into account the heat capacity²⁵ and optical²⁶ data we estimate²⁷ that the surface transient temperature rise due to the photoexcitation is ~ 20 K at $\mathcal{F} = 10 \mu\text{J}/\text{cm}^2$. This is consistent with the observed fluence dependence in EuP-122, where the departure from linearity, that is associated with the destruction of the Eu^{2+} magnetic order at the surface is observed at similar fluences (see Figs. 7 and 8). The departure from linearity is followed by a complete saturation above $\mathcal{F} \sim 50 \mu\text{J}/\text{cm}^2$ where the temperature within the complete probed volume exceeds the magnetic ordering T , as expected from the saturation model²⁸, where the saturation fluence value depends on the geometry and the optical penetration depth of the beams.

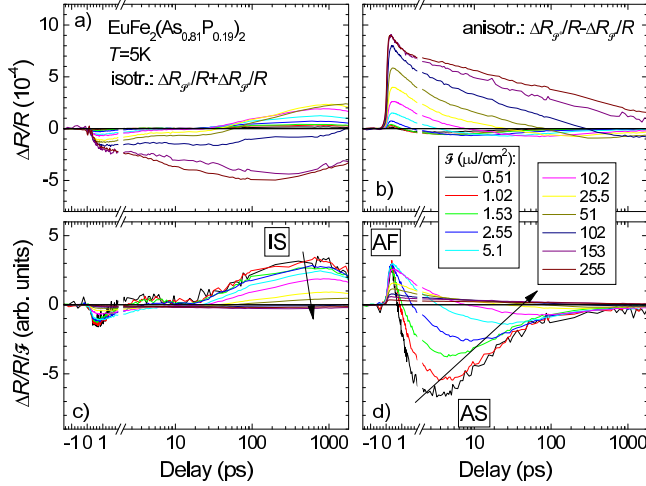


Figure 9. (Color online) The isotropic, (a), and anisotropic, (b), transient components in $\text{EuFe}_2(\text{As}_{0.81}\text{P}_{0.19})_2$ at different fluences obtained from the data shown in Fig. 6. The \mathcal{F} -normalized transients from panels (a) and (b) are shown in (c) and (d), respectively, to emphasize the low- \mathcal{F} region. Arrows indicate the direction of increasing fluence.

In Eu-122 the saturation is, despite the same geometry of the beams, observed above $\mathcal{F} \sim 150 \mu\text{J}/\text{cm}^2$ only, which is ~ 3 times higher than in EuP-122. At this fluence the peak surface lattice temperature is estimated to be $T_{\text{TH}} \sim 70\text{K}$. Deeper in the sample at a probe penetration depth $T_{\text{TH}} \sim 40$ K still significantly exceeds T_{N} . The reason for the difference could be associated with the slower risetime in Eu-122 that prevented us to measure the true amplitude of the response. Instead, the $\Delta R/R$ value at the longest delay was measured, which is still on

the rising part of the signal, and depends on both, the amplitude of the response and the rate of the magnetization suppression. It is reasonable to expect that the rate depends on T_{TH} and as a result on the excitation density also for $T_{\text{TH}} > T_{\text{N}}$.

Let us now focus on the complex fluence dependence of the transients shape in the SC EuP-122. In the absence of an external magnetic field at an intermediate $\mathcal{F} \sim 10 \mu\text{J}/\text{cm}^2$ the slow component appears rather isotropic (see Fig. 3) while the anisotropy was previously¹³ observed only in high magnetic field. The anisotropy of the slow component observed at low excitation fluences in zero magnetic field (see Fig. 8) could therefore be a consequence of an interplay with another anisotropic component that saturates at a rather low \mathcal{F} and is masked by other nonsaturated components at increased \mathcal{F} .

To test this hypothesis we calculate the isotropic part, $(\Delta R/R)_{\text{iso}} = 1/2[(\Delta R/R)_{\mathcal{P}^+} + (\Delta R/R)_{\mathcal{P}^-}]$, and the anisotropic part, $(\Delta R/R)_{\text{an}} = 1/2[(\Delta R/R)_{\mathcal{P}^+} - (\Delta R/R)_{\mathcal{P}^-}]$, of the data shown in Fig. 6 and plot them in Fig. 9.

The slow part of the obtained isotropic (IS) response is below $\mathcal{F} \approx 100 \mu\text{J}/\text{cm}^2$ rather similar to the \mathcal{P}^+ response in Eu-122 and H -parallel responses in high magnetic field¹³ in both samples and it can be associated with the out-of-plane Eu^{2+} demagnetization upon the photoexcitation.

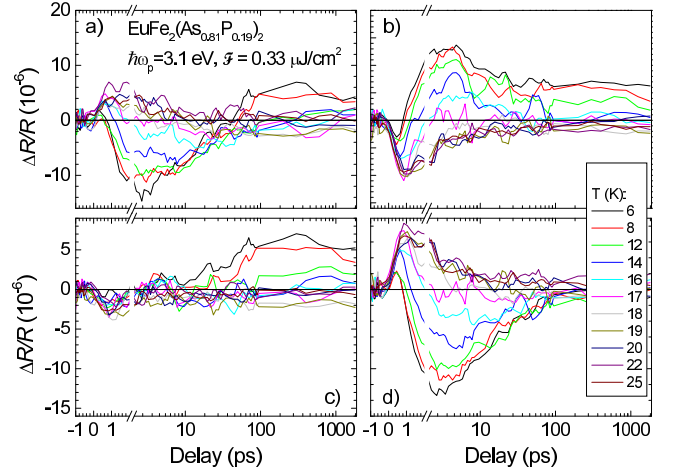


Figure 10. (Color online) Photoinduced reflectivity transients at low T and extremely low \mathcal{F} in EuP-122 for \mathcal{P}^+ (a) and \mathcal{P}^- (b) polarizations. The corresponding isotropic and anisotropic transient components are shown in (c) and (d), respectively. To reduce noise the traces were smoothed resulting in a reduction of the time resolution to ~ 150 fs.

The anisotropic component of the low- \mathcal{F} response is more complex consisting from a fast positive component, marked AF in Fig. 9 (d) and a slower negative component marked AS, which is clearly observed only at low \mathcal{F} .

While component AF can be clearly related to the Fe- d SDW ordering present below $T_{\text{SDW}} \sim 35$ K in our sample the origin of component AS appears more elusive. In $\text{Ba}(\text{Fe},\text{Co})_2\text{As}_2$ a similar slowly relaxing

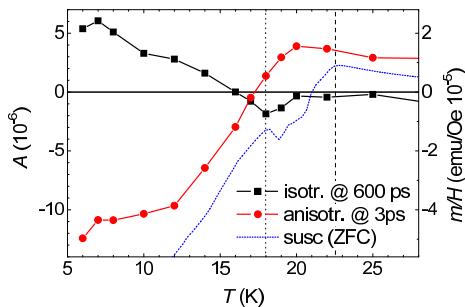


Figure 11. (Color online) Temperature dependence of the amplitudes of the isotropic part at 600-ps delay and the anisotropic part at 3-ps delay from Fig. 10, where the dotted and dashed vertical lines indicate T_{Curie} and T_c (onset) obtained from the susceptibility, respectively. The blue dotted line is the ZFC susceptibility from Fig. 1.

anisotropic response was observed and clearly associated with superconductivity.^{16,29} In optimally doped $\text{Ba}(\text{Fe},\text{Co})_2\text{As}_2$ this SC response is completely saturated above $\mathcal{F}_{\text{sat}} \sim 2 \mu\text{J}/\text{cm}^2$ due to the nonthermal destruction of the SC state,¹⁶ while in underdoped $\text{Ba}(\text{Fe},\text{Co})_2\text{As}_2$ and $\text{Sm}(\text{Fe},\text{Co})\text{AsO}$,³⁰ with lower T_c s, \mathcal{F}_{sat} s are even lower and the magnitudes of the SC response smaller.

Since component AS is similar to a possible anisotropic SC response and the data in Fig. 9 (b) and (d) suggest, that $\mathcal{F}_{\text{sat}}^{\text{AS}}$ is below $0.5 \mu\text{J}/\text{cm}^2$, we measured T dependence also at extremely low $\mathcal{F} = 0.33 \mu\text{J}/\text{cm}^2$ as shown in Fig. 10. Component AS vanishes with increasing T at ~ 20 K [see inset to Fig. 10 (b)], significantly below the bulk T_c (onset) of 22.7 K and rather close to $T_N \sim 18$ K. As a result, despite the similarity of component AS behaviour to the SC response in $\text{Ba}(\text{Fe},\text{Co})_2\text{As}_2$, a firm assignment of component AS to the SC response is not possible. However, in $\text{Sm}(\text{Fe},\text{Co})\text{AsO}$ ³⁰ a similar discrepancy between the bulk T_c and the temperature at which the transient SC component vanishes was observed so a tentative assignment of the SC response to component AS in EuP-122 is plausible.

Component AF, which corresponds to the Fe- d SDW order, shows very similar saturation behaviour to component IS with the linear \mathcal{F} -dependence up to a slightly higher threshold fluence, $\mathcal{F}_c^{\text{SDW}} \sim 20 \mu\text{J}/\text{cm}^2$. This fluence would correspond to a transient lattice heating of $T_{\text{TH}} \sim 25$ K, that is just slightly lower than the equilibrium SDW transition temperature [See Fig. 4 (d)], $T_{\text{SDW}} \sim 35$ K, suggesting almost thermal destruction of the SDW order. However, by taking into account: the fast sub-picosecond \mathcal{F} -independent risetime, a limited accuracy of the transient-heating estimate and the small lattice heat capacity in this T -range the small difference between T_{TH} and T_{SDW} does not imply, that the thermal destruction of the SDW state is more likely than a fast athermal subpicosecond melting of the SDW order.

The relaxation time of component AF increases with

increasing fluence. At low fluences, where the SDW gap is not yet completely suppressed, we attribute it to the bottleneck-governed SDW order recovery dynamics¹⁹, as in the undoped SDW iron pnictides^{16,17,19}. At the fluences near and above the threshold the recovery slows down to tens of picoseconds near the threshold to beyond a few hundred picoseconds at the highest experimental fluence. On this timescales the bottleneck mechanism can not be operative and the nematic lattice-strain dynamics, that was observed recently³¹ to extend to several 100 ps near the magnetostructural transition temperature, might determine the characteristic time scale at these fluences. However, on the nanosecond timescale the heat diffusion out of the experimental volume also takes place. Since no clear evidence for a slow anisotropic dynamics is observed in the low-excitation-density response at higher T , where the nematic fluctuations dominate the response, the timescale is most likely governed by heat diffusion.

IV. SUMMARY AND CONCLUSIONS

Transient optical reflectivity was investigated in $\text{EuFe}_2(\text{As}_{1-x}\text{P}_x)_2$ in the undoped, $x = 0$, SDW and doped, $x = 0.19$, SC state samples as a function of the excitation fluence. The characteristic anisotropic subpicosecond transient reflectivity response indicates the presence of the SDW order below $T_{\text{SDW}} \sim 35$ K also in the $x = 0.19$ SC sample suggesting a *coexistence of Fe- d -SDW, SC and Eu^{2+} -FM orders*. At both dopings a characteristic bottleneck behaviour of the fast picosecond transient reflectivity response due to a partial charge gap present in the SDW state was observed, consistent with previous results.¹⁹

With increasing excitation pulse fluence the saturation of different transient reflectivity components indicates a suppression of the SC order below $\sim 1 \mu\text{J}/\text{cm}^2$, followed by a suppression of the Eu^{2+} -FM order at $\sim 10 \mu\text{J}/\text{cm}^2$ (at $T = 1.5$ K). The SDW order is suppressed in the $x = 0.19$ SC sample at $\sim 20 \mu\text{J}/\text{cm}^2$ while no suppression is evident in the undoped $x = 0$ sample up to $250 \mu\text{J}/\text{cm}^2$.

While the suppression of the Eu^{2+} -FM order appears to be thermal due to the lattice temperature rise above the respective magnetic ordering temperatures, the SDW order suppression in the $x = 0.19$ SC sample is non-thermal with the peak lattice temperature reaching only ~ 10 K below T_{SDW} . The slow thermal suppression of the Eu^{2+} -FM order further confirms the rather weak coupling¹³ of the Eu^{2+} spins to the rest of the system.

ACKNOWLEDGMENTS

Work at Jozef Stefan Institute was supported by ARRS (Grant No. P1-0040). We would like to thank Z. Jaglicic for magnetic susceptibility measurements.

-
- * tomaz.mertelj@ijs.si
- ¹ Y. Kamihara, H. Hiramatsu, M. Hirano, R. Kawamura, H. Yanagi, T. Kamiya, and H. Hosono, *Journal of the American Chemical Society* **128**, 10012 (2006).
 - ² Y. Kamihara, T. Watanabe, M. Hirano, H. Hosono, *et al.*, *J. Am. Chem. Soc.* **130**, 3296 (2008).
 - ³ Z. Ren, Q. Tao, S. Jiang, C. Feng, C. Wang, J. Dai, G. Cao, and Z. Xu, *Physical Review Letters* **102** (2009), 10.1103/PhysRevLett.102.137002.
 - ⁴ S. Jiang, H. Xing, G. Xuan, Z. Ren, C. Wang, Z.-A. Xu, and G. Cao, *Phys. Rev. B* **80**, 184514 (2009).
 - ⁵ P. W. Anderson and H. Suhl, *Phys. Rev.* **116**, 898 (1959).
 - ⁶ A. I. Buzdin, L. N. Bulaevskii, M. L. Kuchik, and S. V. Panyukov, *Soviet Physics Uspekhi* **27**, 927 (1984).
 - ⁷ A. Błachowski, K. Ruebenbauer, J. Żukrowski, Z. Bukowski, K. Rogacki, P. J. W. Moll, and J. Karpinski, *Phys. Rev. B* **84**, 174503 (2011).
 - ⁸ H. S. Jeevan, D. Kasinathan, H. Rosner, and P. Gegenwart, *Phys. Rev. B* **83**, 054511 (2011).
 - ⁹ Z. Ren, Z. Zhu, S. Jiang, X. Xu, Q. Tao, C. Wang, C. Feng, G. Cao, and Z.-A. Xu, *Physical Review B* **78** (2008), 10.1103/PhysRevB.78.052501.
 - ¹⁰ S. Zapf, D. Wu, L. Bogani, H. S. Jeevan, P. Gegenwart, and M. Dressel, *Phys. Rev. B* **84**, 140503 (2011).
 - ¹¹ S. Zapf, H. S. Jeevan, T. Ivek, F. Pfister, F. Klingert, S. Jiang, D. Wu, P. Gegenwart, R. K. Kremer, and M. Dressel, *Physical Review Letters* **110**, 237002 (2013).
 - ¹² S. Nandi, W. T. Jin, Y. Xiao, Y. Su, S. Price, D. K. Shukla, J. Stempfer, H. S. Jeevan, P. Gegenwart, and T. Brückel, *Phys. Rev. B* **89**, 014512 (2014).
 - ¹³ A. Pogrebna, T. Mertelj, N. Vujičić, G. Cao, Z. A. Xu, and D. Mihailovic, *Sci. Rep.* **5**, (2015).
 - ¹⁴ W.-H. Jiao, Q. Tao, J.-K. Bao, Y.-L. Sun, C.-M. Feng, Z.-A. Xu, I. Nowik, I. Felner, and G.-H. Cao, *EPL (Europhysics Letters)* **95**, 67007 (2011).
 - ¹⁵ S. Jiang, Y. Luo, Z. Ren, Z. Zhu, C. Wang, X. Xu, Q. Tao, G. Cao, and Z.-A. Xu, *New Journal of Physics* **11**, 025007 (2009).
 - ¹⁶ L. Stojchevska, T. Mertelj, J. Chu, I. Fisher, and D. Mihailovic, *Physical Review B* **86**, 024519 (2012).
 - ¹⁷ L. Stojchevska, P. Kusar, T. Mertelj, V. V. Kabanov, X. Lin, G. H. Cao, Z. A. Xu, and D. Mihailovic, *Phys. Rev. B* **82**, 012505 (2010).
 - ¹⁸ T. Mertelj, P. Kusar, V. V. Kabanov, L. Stojchevska, N. D. Zhigadlo, S. Katrych, Z. Bukowski, J. Karpinski, S. Weyeneth, and D. Mihailovic, *Phys. Rev. B* **81**, 224504 (2010).
 - ¹⁹ A. Pogrebna, N. Vujičić, T. Mertelj, T. Borzda, G. Cao, Z. A. Xu, J.-H. Chu, I. R. Fisher, and D. Mihailovic, *Phys. Rev. B* **89**, 165131 (2014).
 - ²⁰ Y. Tokiwa, S.-H. Hübner, O. Beck, H. S. Jeevan, and P. Gegenwart, *Phys. Rev. B* **86**, 220505 (2012).
 - ²¹ J.-H. Chu, J. G. Analytis, K. De Greve, P. L. McMahon, Z. Islam, Y. Yamamoto, and I. R. Fisher, *Science* **329**, 824 (2010).
 - ²² J.-H. Chu, J. G. Analytis, D. Press, K. De Greve, T. D. Ladd, Y. Yamamoto, and I. R. Fisher, *Phys. Rev. B* **81**, 214502 (2010).
 - ²³ Duszka, A., Lucarelli, A., Pfuner, F., Chu, J.-H., Fisher, I. R., and Degiorgi, L., *EPL* **93**, 37002 (2011).
 - ²⁴ Y. Xiao, Y. Su, M. Meven, R. Mittal, C. M. N. Kumar, T. Chatterji, S. Price, J. Persson, N. Kumar, S. K. Dhar, A. Thamizhavel, and T. Brueckel, *Physical Review B* **80** (2009), 10.1103/PhysRevB.80.174424.
 - ²⁵ H. S. Jeevan, Z. Hossain, D. Kasinathan, H. Rosner, C. Geibel, and P. Gegenwart, *Phys. Rev. B* **78**, 052502 (2008).
 - ²⁶ D. Wu, N. Barišić, N. Drichko, S. Kaiser, A. Faridian, M. Dressel, S. Jiang, Z. Ren, L. J. Li, G. H. Cao, Z. A. Xu, H. S. Jeevan, and P. Gegenwart, *Phys. Rev. B* **79**, 155103 (2009).
 - ²⁷ We obtain the light penetration depth of $\lambda_{\text{opt}} = 27$ nm at $\hbar\omega = 1.55$ eV .
 - ²⁸ P. Kusar, V. Kabanov, J. Demsar, T. Mertelj, S. Sugai, and D. Mihailovic, *Physical Review Letters* **101**, 227001 (2008).
 - ²⁹ D. H. Torchinsky, J. W. McIver, D. Hsieh, G. F. Chen, J. L. Luo, N. L. Wang, and N. Gedik, *Phys. Rev. B* **84**, 104518 (2011).
 - ³⁰ T. Mertelj, L. Stojchevska, N. D. Zhigadlo, J. Karpinski, and D. Mihailovic, *Phys. Rev. B* **87**, 174525 (2013).
 - ³¹ A. Patz, T. Li, S. Ran, R. M. Fernandes, J. Schmalian, S. L. Bud'ko, P. C. Canfield, I. E. Perakis, and J. Wang, *Nat Commun* **5** (2014).